Appl Phys B (2009) 95: 145–153
DOI 10.1007/s00340-008-3331-9

Applied Physics B
Lasers and Optics

Numerical study of optical properties of InGaN multi-quantum-well laser diodes with polarization-matched AlInGaN barrier layers

J.-R. Chen · S.-C. Ling · H.-M. Huang · P.-Y. Su · T.-S. Ko · T.-C. Lu · H.-C. Kuo · Y.-K. Kuo · S.-C. Wang

Received: 30 September 2008 / Published online: 12 December 2008
© Springer-Verlag 2008

Abstract The optical properties of InGaN multi-quantum-well laser diodes with different polarization-matched AlInGaN barrier layers have been investigated numerically by employing an advanced device simulation program. The use of quaternary polarization-matched AlInGaN barrier layers enhances the electron–hole wave function overlap due to the compensation of polarization charges between InGaN quantum well and AlInGaN barrier layer. According to the simulation results, it is found that, among the polarization-matched quantum-well structures under study, lower threshold current and higher slope efficiency can be achieved simultaneously when the aluminum composition in AlInGaN barrier layers is about 10–15%. The optimal polarization-matched InGaN/AlInGaN laser diode shows lower threshold current and higher slope efficiency compared to conventional InGaN/InGaN laser diodes.

PACS 42.55.Px · 78.20.-e · 78.20.Bh · 78.30.Fs

1 Introduction

Gallium nitride (GaN)-based light-emitting diodes (LEDs) and laser diodes (LDs) have received much attention in the past few years due to their promising applications such as solid-state lighting, high-density optical storage systems, and laser projection displays [1–4]. In order to develop these expected productions, many research groups are devoted to the study of high-performance LEDs and LDs. Although InGaN/GaN laser diodes with an emission wavelength near 405 nm have been commercialized as light sources of the blu-ray disk system and the high-definition digital versatile disk (HD-DVD), superior operation performance and shorter emission wavelength are expected as challenges for the next-generation devices. Recently, several high-performance InGaN-based laser diodes have been achieved. Asano et al. demonstrated 100-mW kink-free blue–violet laser diodes in 2003 [5]. Ultraviolet laser diodes with 350.9-nm lasing wavelength were also realized by Kamiyama et al. in 2005 [6]. Moreover, Ryu et al. demonstrated single-mode blue–violet laser diodes with low beam divergence and high catastrophic optical damage (COD) level in 2006 [7]. They also reported high-performance blue laser diodes with an emission wavelength of 448 nm and a maximum output power of >300 mW in 2007 [8]. Although these high-performance laser diodes were reported, the inherent problem of piezoelectric and spontaneous polarization in *c*-plane GaN-based alloys is one of the most important properties which limit the development of GaN-based optoelectronic devices [9].

Several approaches have been proposed to eliminate, or reduce, the polarization effect in nitride-based heterostructures. Franssen et al. demonstrated that the polarization-induced electric fields can be fully screened by employing heavy 1×10^{19} cm^{-3} Si doping in quantum barriers [10]. Nevertheless, heavy Si doping in quantum barriers will induce severe free-carrier absorption, which results in the increase of laser threshold current. Besides, non-polar (*a* and *m* plane) and semipolar quantum wells are other approaches

J.-R. Chen (✉) · S.-C. Ling · H.-M. Huang · P.-Y. Su · T.-S. Ko · T.-C. Lu · H.-C. Kuo · S.-C. Wang
Department of Photonics & Institute of Electro-Optical Engineering, National Chiao Tung University, Hsinchu 300, Taiwan
e-mail: jrchen.eo95g@nctu.edu.tw
Fax: +886-3-571-6631

Y.-K. Kuo
Department of Physics, National Changhua University of Education, Changhua 500, Taiwan

to this problem [11–14]. However, high dislocation density caused by large lattice mismatch and stacking faults inhibits the related development [15–17]. Recently, the concept of employing polarization-matched quaternary AlInGaN barrier layers has been proposed to control the electrostatic field in the quantum wells, which could be an attractive approach to the problem of the electrostatic field in *c*-plane GaN-based heterostructures. By using quaternary AlInGaN barrier layers, we could control both spontaneous and piezoelectric polarization in the quantum wells as the appropriate aluminum and indium compositions are chosen [18–22].

In order to further investigate the GaN-based laser diodes with polarization-matched AlInGaN barrier layers, systematic and compact theoretical modeling is a necessary approach to improve existing laser structures and understand internal physical processes, which provides timely and efficient guidance toward the optimal structure design and device parameters. In this study, the InGaN laser diodes with different polarization-matched AlInGaN barrier layers are systematically studied in detail by using an advanced laser technology integrated program (LASTIP), which self-consistently combines quantum well band structure calculations by 6×6 $k \cdot p$ theory, radiative and non-radiative carrier recombination, carrier drift and diffusion, and optical mode computation [23]. By appropriately designing the aluminum and indium compositions in AlInGaN barrier layers, the built-in charge density at the interface between InGaN well and AlInGaN barrier layer can be compensated. Under this circumstance, the electron–hole wave function overlap in the InGaN/AlInGaN quantum well increases as compared with the conventional InGaN/GaN or InGaN/InGaN quantum well and thus the performance of the polarization-matched InGaN/AlInGaN quantum-well lasers can be enhanced. Furthermore, how the different physical mechanisms influence the threshold properties is investigated in this study as well.

2 Theoretical method and device structure

The self-consistent LASTIP simulation program combines band-structure and gain calculations with two-dimensional (2-D) simulations of wave guiding, carrier transport, and heat flux. The carrier-transport model includes drift and diffusion of electrons and holes in devices. Built-in polarization induced by spontaneous and piezoelectric polarization is considered at hetero-interfaces of nitride-related devices. In the quantum wells, self-consistent Poisson and Schrödinger equations are recomputed at every bias point for the states of quantum-well levels and carrier distributions. In the optical mode model, a 2-D scalar complex wave equation is solved for the lateral modes. The physical model of the InGaN quantum wells is considered in such a way that the conduction bands are assumed to be decoupled from valence subbands and have isotropic parabolic bands due to the larger band gap of nitride semiconductors and the valence band structures, which include the coupling of the heavy-hole (HH), the light-hole (LH), and the spin–orbit split-off bands, are calculated by the 6×6 Hamiltonian with envelope-function approximation [24, 25]. The optical gain spectra of quantum-well structures, with the valence-band-mixing effect being taken into account, follow the expression in [26], including a Lorentzian broadening function with 0.1-ps scattering time [26–28]. The calculations of carrier capture and escape from the quantum wells are considered in accordance with the model provided by Romero et al. [29]. More description about the physical models utilized in the LASTIP simulation program can be found in [30, 31].

In this simulation, we first assume that the InGaN laser diodes are grown on a 3-μm n-type GaN layer. On top of this GaN layer is a 0.1-μm-thick n-type $In_{0.1}Ga_{0.9}N$ compliant layer and a 1.0-μm-thick n-type $Al_{0.07}Ga_{0.93}N$ cladding layer, followed by a 0.1-μm-thick n-type GaN guiding layer. The multiple-quantum-well active region consists of two 2-nm-thick $In_{0.1}Ga_{0.9}N$ quantum wells and 5-nm-thick $In_{0.035}Ga_{0.965}N$ or AlInGaN barrier layers. A 20-nm-thick p-type $Al_{0.2}Ga_{0.8}N$ electronic blocking layer (EBL) is grown on top of the active region to reduce electron leakage into the p-type GaN layer [32, 33]. Furthermore, a 0.1-μm-thick p-type GaN guiding layer and a 1.0-μm-thick p-type $Al_{0.07}Ga_{0.93}N$ cladding layer are grown. Finally, a 0.1-μm-thick p-type GaN cap layer is grown to complete the structure. The effective active region of the ridge geometry is 2 μm in width and 500 μm in length. The reflectivities of the two end mirrors are set at 20% and 50%, respectively. The doping concentrations in each layer and the detailed device structure are described in Table 1.

3 Material parameters

In order to obtain reliable simulation results, proper material parameters are essential in the physical model. The material parameters of the binary semiconductors required for $k \cdot p$ calculations are taken from the paper by Vurgaftman and Meyer [34] and summarized in Table 2. As for AlInGaN materials, a linear interpolation between the parameters of the relevant binary semiconductors is utilized except for the band-gap energies. For the physical parameter P, the interpolation formula is [35]

$$P(\mathrm{Al}_x\mathrm{In}_y\mathrm{Ga}_{1-x-y}\mathrm{N}) = P(\mathrm{AlN})x + P(\mathrm{InN})y + P(\mathrm{GaN})(1-x-y). \quad (1)$$

The AlInGaN band-gap energies can be expressed as a weighted sum of the band-gap energies of relevant ternary

Table 1 Layer structure and room-temperature physical parameters of the InGaN quantum-well laser under study (d, layer thickness; N_{dop}, doped carrier density; n, refractive index at wavelength 400 nm; κ, thermal conductivity). The doped carrier density, N_{dop}, represents the actual density of free carriers

Parameter (unit)	d (nm)	N_{dop} (1/cm^3)	n	κ (W/cm K)
p-GaN (contact)	100	1×10^{18}	2.55	1.3
p-$Al_{0.07}Ga_{0.93}N$ (cladding)	1000	5×10^{17}	2.519	0.8
p-GaN (waveguide)	100	5×10^{17}	2.55	1.3
p-$Al_{0.2}Ga_{0.8}N$ (EBL)	20	5×10^{17}	2.489	0.8
i-$In_{0.035}Ga_{0.965}N$ (barrier)	5	–	2.585	0.6
i-$In_{0.1}Ga_{0.9}N$ (quantum well)	2	–	3.835	0.5
i-$In_{0.035}Ga_{0.965}N$ (barrier)	5	–	2.585	0.6
i-$In_{0.1}Ga_{0.9}N$ (quantum well)	2	–	3.835	0.5
i-$In_{0.035}Ga_{0.965}N$ (barrier)	5	–	2.585	0.6
n-GaN (waveguide)	100	1×10^{18}	2.55	1.3
n-$Al_{0.07}Ga_{0.93}N$ (cladding)	1000	1×10^{18}	2.519	0.8
n-$In_{0.1}Ga_{0.9}N$ (compliance)	100	1×10^{18}	2.835	0.5
n-GaN (substrate)	3000	1×10^{18}	2.55	1.3

Table 2 Material parameters of the binary semiconductors GaN, AlN, and InN at room temperature ($\Delta_{cr}=\Delta_1$, $\Delta_{so}=3\Delta_2=3\Delta_3$)

Parameter	Symbol (unit)	GaN	AlN	InN
Lattice constant	a_0 (Å)	3.189	3.112	3.545
Spin−orbit split energy	Δ_{so} (eV)	0.017	0.019	0.005
Crystal-field split energy	Δ_{cr} (eV)	0.010	−0.169	0.040
Hole effective mass parameter	A_1	−7.21	−3.86	−8.21
	A_2	−0.44	−0.25	−0.68
	A_3	6.68	3.58	7.57
	A_4	−3.46	−1.32	−5.23
	A_5	−3.40	−1.47	−5.11
	A_6	−4.90	−1.64	−5.96
Hydrost. deform. potential (c axis)	a_z (eV)	−4.9	−3.4	−3.5
Hydrost. deform. potential (transverse)	a_t (eV)	−11.3	−11.8	−3.5
Shear deform. potential	D_1 (eV)	−3.7	−17.1	−3.7
	D_2 (eV)	4.5	7.9	4.5
	D_3 (eV)	8.2	8.8	8.2
	D_4 (eV)	−4.1	−3.9	−4.1
Elastic stiffness constant	C_{33} (GPa)	398	373	224
Elastic stiffness constant	C_{13} (GPa)	106	108	92
Electron effective mass (c axis)	m_e^z/m_0	0.2	0.32	0.07
Electron effective mass (transverse)	m_e^t/m_0	0.2	0.30	0.07

semiconductors with appropriate band-gap bowing parameters. Specifically, the AlInGaN band-gap energies are calculated by the following expressions [36]:

$$E_g(\text{AlInGaN}) = \frac{xyE_g^u(\text{AlInN}) + yzE_g^v(\text{InGaN}) + xzE_g^w(\text{AlGaN})}{xy+yz+zx}, \quad (2)$$

$$E_g^u(\text{AlInN}) = uE_g(\text{InN}) + (1-u)E_g(\text{AlN}) - u(1-u)B(\text{AlInN}), \quad (3)$$

$$E_g^v(\text{InGaN}) = vE_g(\text{GaN}) + (1-v)E_g(\text{InN}) - v(1-v)B(\text{InGaN}), \quad (4)$$

$$E_g^w(\text{AlGaN}) = wE_g(\text{GaN}) + (1-w)E_g(\text{AlN}) - w(1-w)B(\text{AlGaN}), \quad (5)$$

$$u = \frac{1-x+y}{2}, \qquad v = \frac{1-y+z}{2}, \qquad w = \frac{1-x+z}{2}, \tag{6}$$

where x, y, and $z = 1 - x - y$ represent the compositions of aluminum, indium, and gallium in the AlInGaN material system, respectively. The band-gap bowing parameters of AlInN, InGaN, and AlGaN are 2.5 eV, 1.4 eV, and 0.7 eV, respectively [34].

Built-in polarization induced due to spontaneous and piezoelectric polarization is known to influence the performance of nitride devices. In order to consider the built-in polarization within the interfaces of nitride devices, the method developed by Fiorentini et al. is employed to estimate the built-in polarization, which is represented by fixed interface charges at each hetero-interface. They provided explicit rules to calculate the nonlinear polarization for nitride alloys of arbitrary composition [37]. Specifically, the spontaneous polarization of ternary nitride alloys can be expressed by

$$P_{sp}(Al_xGa_{1-x}N) = -0.090x - 0.034(1-x) + 0.019x(1-x), \tag{7}$$

$$P_{sp}(In_xGa_{1-x}N) = -0.042x - 0.034(1-x) + 0.038x(1-x), \tag{8}$$

$$P_{sp}(Al_xIn_{1-x}N) = -0.090x - 0.042(1-x) + 0.071x(1-x). \tag{9}$$

The spontaneous polarization of quaternary AlInGaN can be calculated in a similar way as that shown in expression (2). As for the piezoelectric polarization of AlInGaN, InGaN, and AlGaN, it can be calculated by the following expression:

$$P_{pz}(Al_xIn_yGa_{1-x-y}N) = P_{pz}(AlN)x + P_{pz}(InN)y + P_{pz}(GaN)(1-x-y), \tag{10}$$

where

$$P_{pz}(AlN) = -1.808\varepsilon + 5.624\varepsilon^2 \quad \text{for } \varepsilon < 0, \tag{11}$$

$$P_{pz}(AlN) = -1.808\varepsilon - 7.888\varepsilon^2 \quad \text{for } \varepsilon > 0, \tag{12}$$

$$P_{pz}(GaN) = -0.918\varepsilon + 9.541\varepsilon^2, \tag{13}$$

$$P_{pz}(InN) = -1.373\varepsilon + 7.559\varepsilon^2, \tag{14}$$

$$\varepsilon = (a_{subs} - a_L)/a_L. \tag{15}$$

Here a_{subs} and a_L are the lattice constants of the substrate and epitaxial layer, respectively. The total built-in polarization is the sum of spontaneous and piezoelectric polarization. At an abrupt interface of a top/bottom layer heterostructure such as InGaN/GaN or AlGaN/GaN, the polarization can decrease or increase within a bilayer, causing a fixed polarization charge density σ defined by [38]

$$\sigma(P_{sp} + P_{pz}) = P(\text{bottom}) - P(\text{top}) = [P_{sp}(\text{bottom}) + P_{pz}(\text{bottom})] - [P_{sp}(\text{top}) + P_{pz}(\text{top})]. \tag{16}$$

Table 3 Net surface charge density at each interface of the InGaN laser diode

Interface	Built-in charge density
$Al_{0.07}Ga_{0.93}N/GaN$	$+2.86 \times 10^{12}$ cm^{-2}
$GaN/Al_{0.2}Ga_{0.8}N$	-8.82×10^{12} cm^{-2}
$Al_{0.2}Ga_{0.8}N/In_{0.035}Ga_{0.965}N$	$+1.20 \times 10^{13}$ cm^{-2}
$In_{0.035}Ga_{0.965}N/In_{0.1}Ga_{0.9}N$	$+6.46 \times 10^{12}$ cm^{-2}
$In_{0.1}Ga_{0.9}N/In_{0.035}Ga_{0.965}N$	-6.46×10^{12} cm^{-2}
$In_{0.035}Ga_{0.965}N/GaN$	-3.19×10^{12} cm^{-2}
$GaN/Al_{0.07}Ga_{0.93}N$	-2.86×10^{12} cm^{-2}

For the InGaN quantum-well lasers under study, the net surface charges at all interfaces are calculated and listed in Table 3. Although the interface charges can be obtained by this theoretical model, experimental investigations often find weaker built-in polarization than that predicted by theoretical calculation. It is mainly attributed to partial compensation of the built-in polarization by defect and interface charges [39]. Typical reported experimental values are 20%, 50%, or 80% smaller than the theoretically calculated values [40–42]. As a result, 50% of the theoretical polarization values are used in our simulation from the average of the reported values.

The thermal conductivities of nitride compounds listed in Table 1 are obtained from the values of binary GaN, AlN, and InN by considering the impact of alloy and interface scattering of phonons. In our simulation, the thermal conductivities of GaN, AlN, and InN are 1.3 W/cm K, 2.85 W/cm K, and 0.45 W/cm K, respectively [30]. As for the refractive-index parameter, the Adachi model is employed to calculate the refractive-index values in each layer listed in Table 1 as well [43]. The band-offset ratio, which is defined as the ratio between the conduction-band offset ΔE_c and the valence-band offset ΔE_v, of an InGaN/InGaN quantum well is assumed to be 0.7/0.3 based on the published literature [44, 45].

4 Simulation results and discussion

The spontaneous and piezoelectric polarization charges as a function of Al or In composition for ternary AlGaN and InGaN alloys grown pseudomorphically on GaN templates are plotted in Fig. 1. Since the strains of AlGaN and InGaN epitaxial layers are tensile and compressive respectively as compared with GaN templates, it can be found that

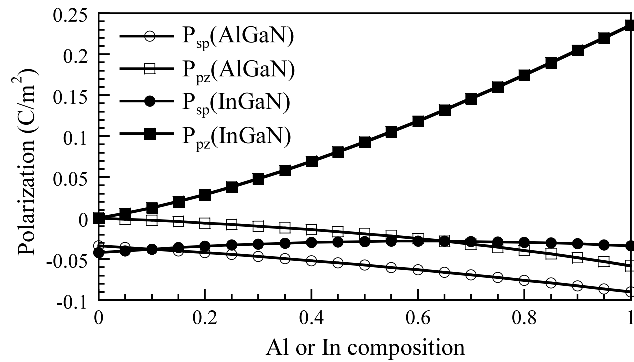

Fig. 1 Spontaneous (P_{sp}) and piezoelectric (P_{pz}) polarization charges as a function of Al or In composition for ternary AlGaN and InGaN alloys grown pseudomorphically on GaN templates

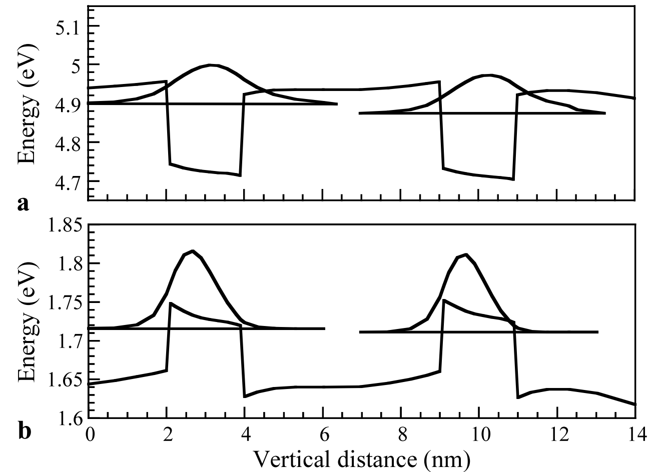

Fig. 2 Potential profiles and the subband wave functions (C1 and HH1) for (**a**) conduction and (**b**) valence band in the active region of the conventional InGaN/InGaN laser diodes at the injection current of 120 mA

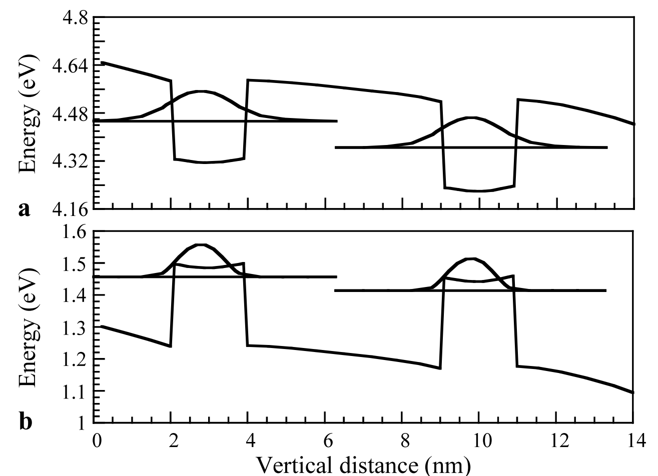

Fig. 3 Potential profiles and the subband wave functions (C1 and HH1) for (**a**) conduction and (**b**) valence band in the active region of the laser diode with polarization-matched $Al_{0.25}In_{0.226}Ga_{0.524}N$ barrier layers at the injection current of 120 mA

the variation of the piezoelectric polarization of AlGaN and InGaN is opposite with increasing Al or In composition. Although the spontaneous polarizations of AlGaN and InGaN, and the piezoelectric polarization of AlGaN, are all negative with increasing Al and In compositions, the obvious increase of the piezoelectric polarization of InGaN with increasing In compositions could compensate the total polarizations. Therefore, by employing appropriate Al and In compositions in the AlInGaN barrier layers, it can be found that the polarizations at the interface between InGaN quantum wells and AlInGaN barrier layers can be matched according to the results of theoretical calculation [20, 22, 37]. The Al and In compositions are determined by fixing a specific Al composition and varying the In composition to find the minimum interface charge density. When different Al compositions are chosen, there are corresponding In compositions which make the InGaN/AlInGaN interface charge density minimum. Therefore, several different Al and In compositions can reach this requirement. For comparison purposes, $Al_{0.25}In_{0.226}Ga_{0.524}N$ is chosen to be the polarization-matched quaternary barrier layer in our preliminary study because its energy band gap is nearly identical to that of the original $In_{0.035}Ga_{0.965}N$ barrier layer after considering the strain-induced band-gap variation in both barrier layers. The interface charge density between the $In_{0.1}Ga_{0.9}N$ quantum well and the $Al_{0.25}In_{0.226}Ga_{0.524}N$ barrier layer is $3.12 \times 10^{10}\ \mathrm{cm}^{-2}$. This value is dramatically reduced as compared with that of the conventional InGaN barrier layer, as shown in Table 3. In Fig. 2 we depict the potential profiles and the subband wave functions (C1 and HH1) for (a) conduction and (b) valence band in the active region of the conventional InGaN/InGaN laser diodes at the injection current of 120 mA. Data shown in Fig. 2 reveal that the built-in electric field causes a strong deformation of the quantum wells and induces a spatial separation of the electron and hole wave functions, which leads to a reduction in the photon emission [9]. Figure 3 shows the potential profiles and the subband wave functions (C1 and HH1) for (a) conduction and (b) valence band in the active region of the laser diode with polarization-matched $Al_{0.25}In_{0.226}Ga_{0.524}N$ barrier layers at the injection current of 120 mA. It is obvious that the relatively flat quantum-well band profiles enhance the electron–hole spatial overlap and consequently increase the oscillator strength and radiative efficiency. Furthermore, to compare the optical properties of these two laser diodes we illustrate the light-output power of the conventional InGaN/InGaN and polarization-matched InGaN/AlInGaN laser diodes as a function of the input current in Fig. 4. It is found that although the threshold current of the laser diode with the quaternary barrier layer is lower than that of the conventional laser diode, the slope efficiency

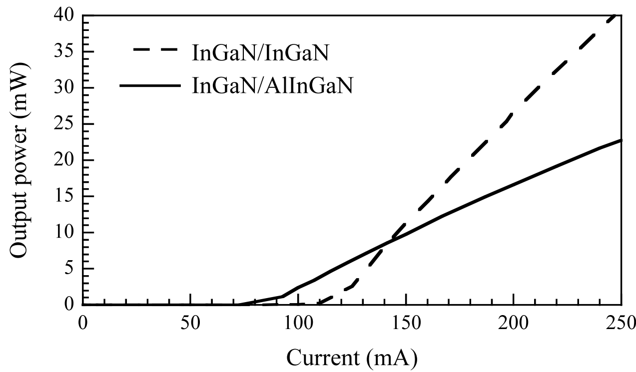

Fig. 4 Light-output power of the conventional InGaN/InGaN and polarization-matched InGaN/AlInGaN laser diodes as a function of the input current

of the polarization-matched laser diode is relatively lower than that of the InGaN/InGaN laser diode.

In order to further understand the internal physical mechanisms which result in the lower slope efficiency in the polarization-matched laser diode, the vertical profiles of electron concentration distribution and conduction band edge in the active region at 120-mA injection current are shown in Fig. 5 for laser structures with InGaN and AlInGaN barrier layers, respectively. In Fig. 5a, it is noteworthy that the effective energy barrier height (i.e. the energy difference between the quasi-Fermi level and the $Al_{0.2}Ga_{0.8}N$ EBL) created by the $Al_{0.2}Ga_{0.8}N$ EBL is substantially reduced by the high density of positive polarization charges at the interface between the InGaN barrier layer and the $Al_{0.2}Ga_{0.8}N$ EBL. Under this condition, the electrons are attracted by Coulomb force and accumulate at this interface, which leads to strong band bending and decreases the effective energy barrier height. Consequently, the increase of laser threshold current will be expected due to the potential tilt in the quantum well and the enhanced electron carrier leakage from the active layer to the p-type cladding layer. On the other hand, we found that this band bending is severer after replacing the InGaN barrier layer with the polarization-matched $Al_{0.25}In_{0.226}Ga_{0.524}N$ barrier layer due to the increase of positive polarization charges. Therefore, the condition of electron accumulation is more obvious and the effective energy barrier height also decreases, as shown in Fig. 5b. Besides, the heterobarrier induced due to the increase of negative charges at the interface between GaN waveguide layer and AlInGaN barrier layer inhibits carrier injection. These factors lead to the strongly non-uniform carrier distribution in two quantum wells of the InGaN/AlInGaN laser diode.

Although the polarization-matched $Al_{0.25}In_{0.226}Ga_{0.524}N$ barrier layer can provide lower threshold current, the decrease of slope efficiency should be improved in the further study. Therefore, other

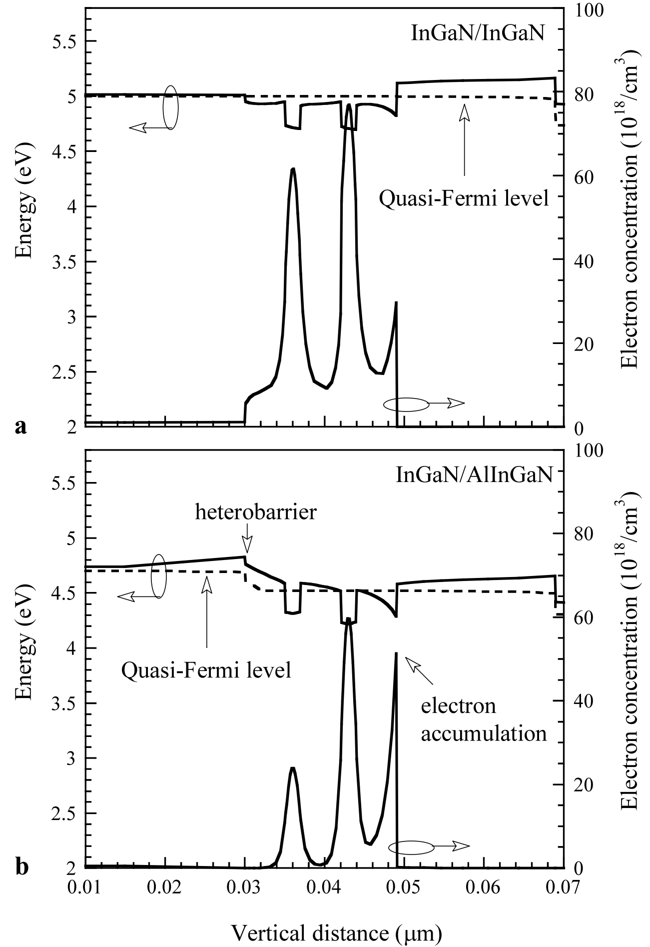

Fig. 5 Vertical profiles of electron concentration distribution and conduction band edge in the active region of the laser structures with (**a**) InGaN and (**b**) AlInGaN barrier layers respectively at 120-mA injection current

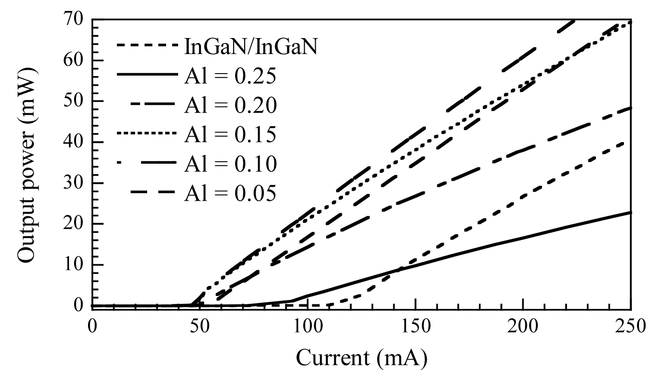

Fig. 6 Light-output power of the conventional and polarization-matched laser diodes as a function of the input current

polarization-matched AlInGaN barrier layers which include $Al_{0.20}In_{0.207}Ga_{0.593}N$, $Al_{0.15}In_{0.188}Ga_{0.662}N$, $Al_{0.10}In_{0.169}Ga_{0.731}N$, and $Al_{0.05}In_{0.150}Ga_{0.80}N$ are employed in our study. Figure 6 shows the light-output power

of the conventional and polarization-matched laser diodes as a function of the input current. The Al composition represents different polarization-matched AlInGaN barrier layers. According to the simulation results, the slope efficiency increases and the threshold current decreases with lower Al composition in AlInGaN barrier layers. However, when the Al composition decreases to 5%, the threshold current becomes higher. Therefore, the optimal Al composition in the AlInGaN barrier layer is about 10–15%. In order to further understand the physical mechanism which leads to the increase of slope efficiency with lower Al composition in AlInGaN barrier layers, the vertical profiles of electron concentration distribution and conduction band edge in the active region at 120-mA injection current are shown in Fig. 7 for laser diodes with polarization-matched (a) $Al_{0.15}In_{0.188}Ga_{0.662}N$ and (b) $Al_{0.05}In_{0.150}Ga_{0.80}N$ barrier layers, respectively. In Fig. 7a, although the electron accumulation still can be found at the interface between barrier layer and EBL, the lower energy band gap resulting from the decreasing Al composition in the AlInGaN barrier layer makes the higher effective energy barrier height in the interface between barrier layer and EBL. Therefore, the electron carrier leakage can be suppressed, which enhances carrier confinement in the active region and also improves the slope efficiency and threshold properties. Moreover, as for the laser diode with the $Al_{0.05}In_{0.150}Ga_{0.80}N$ barrier layer, although the low Al composition in the barrier layer can provide a higher effective energy barrier, it is difficult to provide sufficient carrier confinement in the shallow quantum well, which leads to the electrons spreading into the barrier layer, as shown in Fig. 7b. Lower carrier concentration confined within the quantum well will result in the decrease of recombination efficiency. Therefore, the threshold current increases and the slope efficiency decreases for the laser diodes with the $Al_{0.05}In_{0.150}Ga_{0.80}N$ barrier layer, as shown in Fig. 6. In order to observe the condition of electron leakage current in the laser diodes with different polarization-matched barrier layers, we depict the vertical electron current density profiles within the active regions of laser structures with $Al_{0.25}In_{0.226}Ga_{0.524}N$, $Al_{0.15}In_{0.188}Ga_{0.662}N$, and $Al_{0.05}In_{0.150}Ga_{0.80}N$ barrier layers respectively at 120-mA injection current in Fig. 8a. This driving current is chosen to be above the threshold current values of the laser diodes under study. The positions of two quantum wells are marked with gray areas. The left-hand

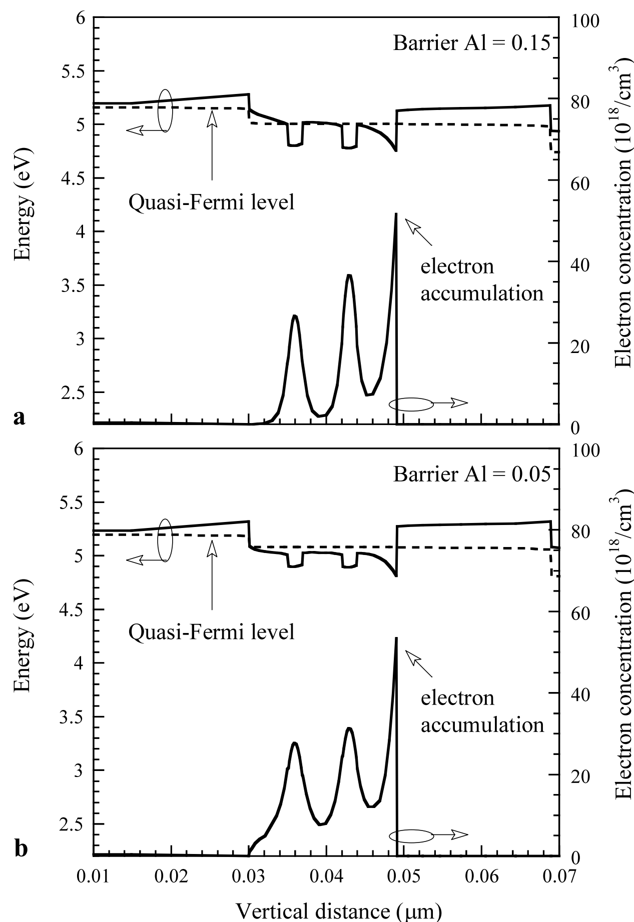

Fig. 7 Vertical profiles of electron concentration distribution and conduction band edge in the active region of the laser structures with polarization-matched (**a**) $Al_{0.15}In_{0.188}Ga_{0.662}N$ and (**b**) $Al_{0.05}In_{0.150}Ga_{0.80}N$ barrier layers respectively at 120-mA injection current

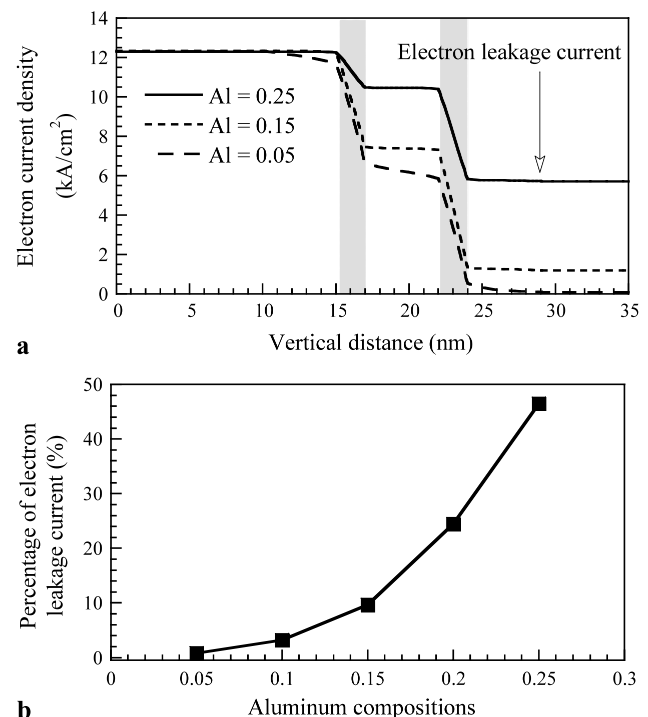

Fig. 8 (**a**) Vertical electron current density profiles within the active regions of laser structures with $Al_{0.25}In_{0.226}Ga_{0.524}N$, $Al_{0.15}In_{0.188}Ga_{0.662}N$, and $Al_{0.05}In_{0.150}Ga_{0.80}N$ barrier layers respectively at 120-mA injection current. (**b**) Percentage of electronic leakage current as a function of the Al compositions in AlInGaN barrier layer at 120-mA injection current

side of the figure is the n-side of the device. The electron current is injected from n-type layers into quantum wells and recombines with holes in quantum wells. Therefore, the electron current density is reduced in the quantum wells. Electron current which overflows through quantum wells is viewed as leakage current. The problem of electron leakage current plays an important role for the optical performance of III-nitride laser diodes [32, 33]. In Fig. 8a, electron leakage current is severe for the laser diode with the $Al_{0.25}In_{0.226}Ga_{0.524}N$ barrier layer. Although the higher Al composition in the barrier layer creates a deeper quantum well, the effective energy barrier provided by EBL is relatively lower. Therefore, the slope efficiency of the laser diode with the $Al_{0.25}In_{0.226}Ga_{0.524}N$ barrier layer is lower than the conventional laser diodes due to the increase of electron leakage current. Lower Al composition in the AlInGaN barrier layer will create a higher effective energy barrier in the interface between EBL and barrier layer, which can reduce the electron leakage current, as shown in Fig. 8a. Figure 8b depicts the percentage of electronic leakage current as a function of the Al compositions in the AlInGaN barrier layer at 120-mA injection current. The percentage of electron leakage current is defined as the ratio of the electron current overflowed to the p-type layer to that injected into the active region of the laser diodes. It is found that the percentage of electron leakage current increases obviously with the Al composition in AlInGaN barrier layers.

Except for the effects of electron leakage current, the quantum-well optical confinement factor also plays an important role for the laser threshold properties. As the Al and In compositions are changed in the AlInGaN barrier layers, the refractive index will be changed simultaneously. Figure 9 depicts the quantum-well optical confinement factor as a function of the Al compositions in the AlInGaN barrier layers. As shown in Fig. 9, the quantum-well optical confinement factor decreases with the increasing aluminum composition in the AlInGaN barrier layer due to the smaller difference of refractive index between barrier layer and waveguide layer. Therefore, the quantum-well optical confinement factor is also one of the mechanisms which result in the increase of the threshold current with increasing Al composition in the AlInGaN barrier layers.

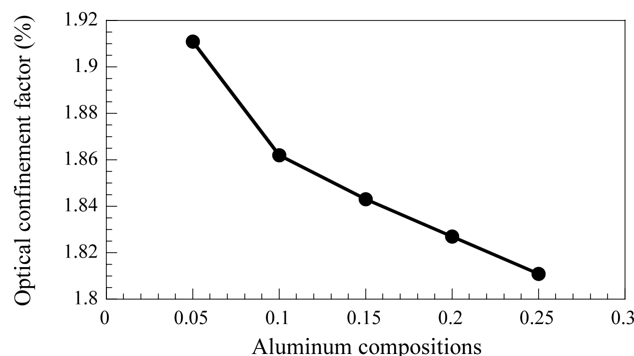

Fig. 9 Quantum-well optical confinement factor as a function of the Al compositions in the AlInGaN barrier layers

5 Conclusion

We have carried out a theoretical simulation to investigate the properties of multi-quantum-well laser diodes with polarization-matched InGaN/AlInGaN quantum-well structures rather than the conventional InGaN/InGaN structures. It is found that although the polarization-matched AlInGaN barrier layers enhance the electron–hole wave function overlap, the strong band bending at the interface between barrier layer and EBL lowers the effective energy barrier height and then results in severe electron leakage current. Furthermore, we decrease the Al compositions in polarization-matched AlInGaN barrier layers. The lower Al composition in a barrier layer provides a higher effective energy barrier height at the interface between barrier layer and EBL, which inhibits the electron leakage current. Moreover, the quantum-well optical confinement factor decreases with the increasing aluminum composition in the AlInGaN barrier layer. The simulation results indicate that, among the polarization-matched quantum-well structures under study, lower threshold current and higher slope efficiency can be achieved simultaneously when the aluminum composition in AlInGaN barrier layers is about 10–15%. The optimal polarization-matched InGaN/AlInGaN laser diode shows superior device performance compared to conventional InGaN/InGaN laser diodes.

Acknowledgements This work was supported in part by the MOE ATU program and in part by the National Science Council of the Republic of China under Contracts NSC 96-2221-E009-092-MY3, NSC 96-2221-E009-093-MY3, NSC 96-2221-E009-094-MY3, and NSC 96-2112-M-018-007-MY3.

References

1. E.F. Schubert, J.K. Kim, Science **308**, 1274 (2005)
2. D.A. Steigerwald, J.C. Bhat, D. Collins, R.M. Fletcher, M.O. Holcomb, M.J. Ludowise, P.S. Martin, S.L. Rudaz, IEEE J. Sel. Top. Quantum Electron. **8**, 310 (2002)
3. S. Nakamura, G. Fasol, *The Blue Laser Diode* (Springer, Berlin, 1997)
4. S. Nakamura, M. Senoh, S. Nagahama, N. Iwasa, T. Matsushita, T. Mukai, Appl. Phys. Lett. **76**, 22 (2000)
5. T. Asano, T. Tojyo, T. Mizuno, M. Takeya, S. Ikeda, K. Shibuya, T. Hino, S. Uchida, M. Ikeda, IEEE J. Quantum Electron. **39**, 135 (2003)
6. S. Kamiyama, K. Iida, T. Kawashima, H. Kasugai, S. Mishima, A. Honshio, Y. Miyake, M. Iwaya, H. Amano, I. Akasaki, IEEE J. Sel. Top. Quantum Electron. **11**, 1069 (2005)
7. H.Y. Ryu, H. Ha, S.N. Lee, K.K. Choi, T. Jang, J.K. Son, J.H. Chae, S.H. Chae, H.S. Paek, Y.J. Sung, T. Sakong, H.G. Kim, K.S. Kim, Y.H. Kim, O.H. Nam, Y.J. Park, IEEE Photon. Technol. Lett. **18**, 1001 (2006)

8. H.Y. Ryu, K.H. Ha, S.N. Lee, T. Jang, J.K. Son, H.S. Paek, Y.J. Sung, H.K. Kim, K.S. Kim, O.H. Nam, Y.J. Park, J.I. Shim, IEEE Photon. Technol. Lett. **19**, 1717 (2007)
9. L.H. Peng, C.W. Chuang, L.H. Lou, Appl. Phys. Lett. **74**, 795 (1999)
10. G. Franssen, T. Suski, P. Perlin, R. Bohdan, A. Bercha, W. Trzeciakowski, I. Makarowa, P. Prystawko, M. Leszczyński, I. Grzegory, S. Porowski, S. Kokenyesi, Appl. Phys. Lett. **87**, 041109 (2005)
11. M.D. Craven, S.H. Lim, F. Wu, J.S. Speck, S.P. DenBaars, Appl. Phys. Lett. **81**, 469 (2002)
12. P. Waltereit, O. Brandt, A. Trampert, H.T. Grahn, J. Menniger, M. Ramsteiner, M. Reiche, K.H. Ploog, Nature **406**, 865 (2000)
13. X. Ni, Ü. Özgür, A.A. Baski, H. Morkoç, L. Zhou, D.J. Smith, C.A. Tran, Appl. Phys. Lett. **90**, 182109 (2007)
14. R. Sharma, P.M. Pattison, H. Masui, R.M. Farrell, T.J. Baker, B.A. Haskell, F. Wu, S.P. DenBaars, J.S. Speck, S. Nakamura, Appl. Phys. Lett. **87**, 231110 (2005)
15. H. Yu, L.K. Lee, T. Jung, P.C. Ku, Appl. Phys. Lett. **90**, 141906 (2007)
16. T. Paskova, R. Kroeger, S. Figge, D. Hommel, V. Darakchieva, B. Monemar, E. Preble, A. Hanser, N.M. Williams, M. Tutor, Appl. Phys. Lett. **89**, 051914 (2006)
17. A. Chakraborty, K.C. Kim, F. Wu, J.S. Speck, S.P. DenBaars, U.K. Mishra, Appl. Phys. Lett. **89**, 041903 (2006)
18. M.A. Khan, J.W. Yang, G. Simin, R. Gaska, M.S. Shur, H.-C. Loye, G. Tamulaitis, A. Zukauskas, D.J. Smith, D. Chandrasekhar, R.B. Tassius, Appl. Phys. Lett. **76**, 1161 (2000)
19. J. Zhang, J. Yang, G. Simin, M. Shatalov, M.A. Khan, M.S. Shur, R. Gaska, Appl. Phys. Lett. **77**, 2668 (2000)
20. M.-H. Kim, M.F. Schubert, Q. Dai, J.K. Kim, E.F. Schubert, J. Piprek, Y. Park, Appl. Phys. Lett. **91**, 183507 (2007)
21. A. Knauer, H. Wenzel, T. Kolbe, S. Einfeldt, M. Weyers, M. Kneissl, G. Tränkle, Appl. Phys. Lett. **92**, 191912 (2008)
22. M.F. Schubert, J. Xu, J.K. Kim, E.F. Schubert, M.H. Kim, S. Yoon, S.M. Lee, C. Sone, T. Sakong, Y. Park, Appl. Phys. Lett. **93**, 041102 (2008)
23. LASTIP (Crosslight Software, Inc., Burnaby, BC, Canada, 2005). http://www.crosslight.com
24. S.L. Chuang, C.S. Chang, Phys. Rev. B **54**, 2491 (1996)
25. S.L. Chuang, C.S. Chang, Appl. Phys. Lett. **68**, 1657 (1996)
26. S.L. Chuang, IEEE J. Quantum Electron. **32**, 1791 (1996)
27. Y.C. Yeo, T.C. Chong, M.-F. Li, W.J. Fan, IEEE J. Quantum Electron. **34**, 526 (1998)
28. Y.C. Yeo, T.C. Chong, M.F. Li, W.J. Fan, J. Appl. Phys. **84**, 1813 (1998)
29. B. Romero, J. Arias, I. Esquivias, M. Cada, Appl. Phys. Lett. **76**, 1504 (2000)
30. J. Piprek, *Semiconductor Optoelectronic Devices: Introduction to Physics and Simulation* (Academic, San Diego, 2003)
31. LASTIP User's Manual Version 2005.11, 1st edn. (Crosslight Software, Burnaby, BC, Canada, 2005)
32. K. Domen, R. Soejima, A. Kuramata, T. Tanahashi, MRS Internet J. Nitride Semicond. Res. **3**, 2 (1998)
33. Y.-K. Kuo, Y.-A. Chang, IEEE J. Quantum Electron. **40**, 437 (2004)
34. I. Vurgaftman, J.R. Meyer, J. Appl. Phys. **94**, 3675 (2003)
35. J. Minch, S.H. Park, T. Keating, S.L. Chuang, IEEE J. Quantum Electron. **35**, 771 (1999)
36. I. Vurgaftman, J.R. Meyer, L.R. Ram-Mohan, J. Appl. Phys. **89**, 5815 (2001)
37. V. Fiorentini, F. Bernardini, O. Ambacher, Appl. Phys. Lett. **80**, 1204 (2002)
38. O. Ambacher, B. Foutz, J. Smart, J.R. Shealy, N.G. Weimann, K. Chu, M. Murphy, A.J. Sierakowski, W.J. Schaff, L.F. Eastman, R. Dimitrov, A. Mitchell, M. Stutzmann, J. Appl. Phys. **87**, 334 (2000)
39. J.P. Ibbetson, P.T. Fini, K.D. Ness, S.P. DenBaars, J.S. Speck, U.K. Mishra, Appl. Phys. Lett. **77**, 250 (2000)
40. S.F. Chichibu, A.C. Abare, M.S. Minsky, S. Keller, S.B. Fleischer, J.E. Bowers, E. Hu, U.K. Mishra, L.A. Coldren, S.P. DenBaars, T. Sota, Appl. Phys. Lett. **73**, 2006 (1998)
41. H. Zhang, E.J. Miller, E.T. Yu, C. Poblenz, J.S. Speck, Appl. Phys. Lett. **84**, 4644 (2004)
42. F. Renner, P. Kiesel, G.H. Dőhler, M. Kneissl, C.G. Van de Walle, N.M. Johnson, Appl. Phys. Lett. **81**, 490 (2002)
43. T. Peng, J. Piprek, Electron. Lett. **32**, 2285 (1996)
44. S.-H. Wei, A. Zunger, Appl. Phys. Lett. **69**, 2719 (1996)
45. Y.-K. Kuo, B.-T. Liou, M.-L. Chen, S.-H. Yen, C.-Y. Lin, Opt. Commun. **231**, 395 (2004)